

RADNet: Ensemble Model for Robust Glaucoma Classification in Color Fundus Images

Dmitrii Medvedev*, Rand Muhtaseb*, and Ahmed Al Mahrooqi*

Mohamed bin Zayed University of Artificial Intelligence
Abu Dhabi, UAE

{dmitrii.medvedev,rand.muhtaseb,ahmed.mahrooqi}@mbzuai.ac.ae

Abstract. Glaucoma is one of the most severe eye diseases, characterized by rapid progression and leading to irreversible blindness. It is often the case that pathology diagnostics is carried out when the one’s sight has already significantly degraded due to the lack of noticeable symptoms at early stage of the disease. Regular glaucoma screenings of the population shall improve early-stage detection, however the desirable frequency of etymological checkups is often not feasible due to excessive load imposed by manual diagnostics on limited number of specialists. Considering the basic methodology to detect glaucoma is to analyze fundus images for the *optic-disc-to-optic-cup ratio*, Machine Learning domain can offer sophisticated tooling for image processing and classification. In our work, we propose an advanced image pre-processing technique combined with an ensemble of deep classification networks. Our *Retinal Auto Detection (RADNet)* model has been successfully tested on Rotterdam EyePACS AIROGS train dataset with AUC of 0.92, and then additionally fine-tuned and tested on a fraction of RIM-ONE DL dataset with AUC of 0.91.

Keywords: Glaucoma Classification · Color Fundus Images · Computer Aided Diagnosis.

1 Introduction

Glaucoma is an eye disease which is considered the leading cause of blindness. It is caused by an increased pressure in the eyes, clinically known as *intraocular pressure (IOP)*, which damages the optic nerve. Patients with glaucoma do not usually experience apparent symptoms, as such, it is referred to as the “silent thief of sight” [14]. A study by Ronan Conlon et al. [4] projected 80 million cases of glaucoma worldwide by the year 2020. Another recent study says that by the year 2040, 111.8 million people will be affected by this disease [1]. Among many types of glaucoma, there are two common types, specified by the structural nature of the disease: *angle closure glaucoma (ACG)* and *open angle glaucoma (OAG)*. The formal type is more common, while the latter progresses much faster to complete blindness with no early intervention. While measuring the IOP may sometimes

* Equal contribution.

help clinicians in diagnosis, it is difficult to accurately take readings due to the unstable nature of optical pressure. Clinicians have resorted to examining the structure and appearance of *optic disc (OD)*, such as the increase of the *cup-to-disc ratio (CDR)* [14]: the ratio of the optic cup diameter to the diameter of the OD. However, manual examination is time-consuming operation and is a subject to the availability of a specialist.

In order to release ophthalmologists from the burden of manual glaucoma screening, multiple automated approaches involving deep learning techniques are explored [2]. This became possible due to the explosive growth of number of deep CNNs architectures for image processing and classification in 2010 [13,25,24,3,11,27,19,10,23,28], as well as the increase of the number of publicly available datasets for glaucoma detection [12].

In this paper, we propose RADNet: a combined methodology of sophisticated image pre-processing and robust ensemble architecture for glaucoma classification. Our model was trained and tested on AIROGS train dataset which accounts for approximately 101k RGB color fundus images of different quality and resolution, mimicking real life conditions of eye screenings. Here, the statement "real life conditions" shall account for camera type and vendor, lighting conditions, presence of patient's tremor during a photo shoot, etc. And in order for our model to produce consistent and robust results regardless of the aforesaid conditions, we introduced a localization of the area of interest with the following pre-processing of this area. RADNet is trained to impose bounding boxes around the OD with a certain padding, and then to apply multiple random affine (translation, scaling, rotation, flips) and non-linear (polar) transformations, as well as such image processing techniques as *Contrast Limited Adaptive Histogram Equalization (CLAHE)* to enhance the classification results. Overall, we have validated eight models during over 150 experiments, and combined three best performing models in ensemble manner. Our proposed methodology allowed us to achieve AUC of 0.92 on a test dataset.

2 Related Works

Glaucoma related research is mainly focused on automated methods of disease screening and segmentation of the *optic disc (OD)* and its outer area with the following classification of referable/no-referable glaucoma. The above mentioned OD and its outer area are traditionally utilized in manual diagnostics, that is why significant amount of published research papers focus on automated extraction of those features. For example, Dibia et al. in [5] proposed to extract from segmented OD such features of eye fundus images as optic disc area, cup diameter, rim area and other important features to calculate *then Cup-to-disc ratio (CDR)*, which is commonly used as an indicator of glaucoma. Even-though the proposed methodology has a strong logical foundation, it was tested on a rather small dataset and may be sensitive to the quality of fundus images collected in real life conditions.

Also, many research papers introduce deep-learning based methods to classify glaucoma. Lee et al. in [15] proposed fully automated CNN based methodology to segment OD and *optic cup (OC)*. The authors modified M-Net, which is a variation of U-Net architecture, for OD detection, limiting the preprocessing of the images to resizing only. The series of experiments on OD segmentation revealed the sensitivity of the results to the quality of images and even the camera’s vendors. For the glaucoma classification task, the team used pretrained ResNet50 and affine transformations for image preprocessing, achieving AUC of 0.96. However, these results were achieved on REFUGE dataset, accounting for 1200 images equally split into train/val/test with glaucoma images accounting for 10% of each part.

Similar approach of 2-step glaucoma screening was presented by Sreng et al. [22], suggesting to segment OD using DeepLabv3, and then classify for glaucoma trying various deep CNNs: AlexNet, GoogleNet, InceptionV3, XceptionNet, ResNet50, SqueezeNet, ShuffleNet, MobileNet, DenseNet, InceptionResNet, NasNet-Large. The authors worked with several datasets (REFUGE, RIM-ONE, ACRIMA, ORGA, DRISTI-GS1) and achieved promising results, but faced some limitations when trying to generalize between datasets. Another limitation was related to the quality of images which in real screening setting can be lower than expected by the model. Maadi et al. in [16] followed the same segment-and-classify approach. As a novelty, the authors modified classical U-Net model, introducing pre-trained SE-ResNet50 on the encoding layers. This allowed to achieve AUC of 0.939 on the above mentioned REFUGE dataset, as well as 0.94 AUC on DRISTI-GS1 (101 images). Moderate sizes and significant imbalance of datasets suggest farther study of generalization capabilities of proposed architecture.

Most recent papers on glaucoma detection continue developing 2-stage process, however it became clear that the first stage in the screening - the image pre-processing and OD segmentation as its sub-field, shall be the focal point of the research, as the major part of successful detection depends of the proper input to a classifier. In line with this idea, Phasuk et al. in [18], proposed an improvements of disk-aware ensemble network (DENet) which incorporates the information from general fundus image with the information from optic disk area. Particularly, the architecture includes two networks for segmentation of OD and OC, and four networks for glaucoma classification. Overall, such structure allowed to achieve AUC of 0.94 on a combined test set from RIM-ONE-R3 (total of 159 stereo images) and DRISHTI-GS (total of 101 images) was used, even though the authors do not specify the train/test split ratio, making their results irreproducible. As another example of deep learning approach, Panda et al. in [17] developed new CNN GlaucoNet to automatically segment OD and OC areas. GlaucoNet relies on extensive patch training to be able to relate borderline pixels either to OD or to OC. Due to the small sizes of used datasets (DRISHTI-GS containing 101 images, RIM-ONE containing 169 images and ORIGA with 650 images), the authors did not employ deep learning for the task of classification, instead taking the classical approach to calculate CDR.

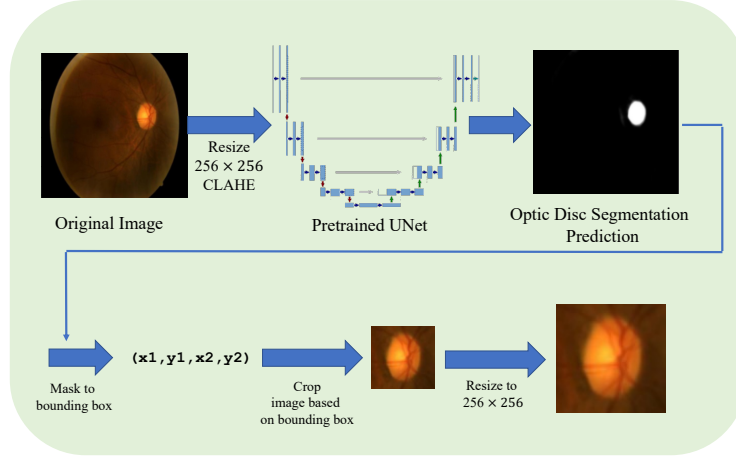


Fig. 1. Preprocessing pipeline used in our experiments on the AIROGS dataset to crop the regions of interest from the original images.

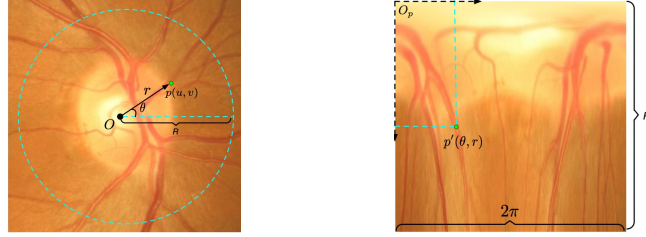


Fig. 2. **Left:** Optic disc area in polar coordinates. **Right:** Transformed image in Cartesian coordinates. Image obtained from [7].

3 Method

3.1 Preprocessing

The AIROGS dataset [26] used in our experiments have non-uniform dimensions. We therefore begin by resizing all images to a fixed dimension of 256×256 pixels, as the pretrained model we will use in the next step was trained on this dimension. In addition, we apply *Contrast Limited Adaptive Histogram Equalization (CLAHE)* before feeding our images into the segmentation model, as this was a preprocessing step used in the pretrained model. We then feed our resized images to a U-Net model pretrained on optic disc segmentation [21] using the RIM-ONE v3 dataset [9] of color fundus images. The generated optic disc segmentation masks are then converted to bounding box coordinates, followed by adding padding to the generated box. The padding value is determined by taking 30% of optic disc's diameter from the segmentation mask. If this number is less than a preset threshold value of 20 pixels, we default the padding value to

20 pixels to ensure a significant padding is added to the bounding box. We then proceed with cropping the original image based on the values of the bounding box coordinates, and finally resize the cropped image to a uniform dimension of 256×256 pixels. In the case where the pretrained network fails to segment the optic disc, or returns a segmentation mask that occupies the majority of the original image, we default by taking a center crop of size 272 pixels followed by an image resize to 256×256 pixels. This represents approximately 20% of our dataset. Since our dataset does not contain segmentation labels of the optic disc, we resort to visually inspect a random set of images to verify the quality of the preprocessing step. The choice of hyperparameters in this stage were determined experimentally by visualizing the produced images. Figure 1 illustrates our overall preprocessing pipeline.

3.2 Ensemble Classification Model

Our glaucoma classification model, RADNet, is composed of an ensemble of three different convolutional neural networks (CNNs) trained on different views of the color fundus images, as illustrated in Figure 3. The first network is trained on the original resized images, whereas the second network is trained on the cropped disc area generated from the preprocessing step, and finally, the third network is trained on the polar transformed cropped images. The training of each model is done independently. As discussed in the upcoming section, we perform a 5-fold cross validation on each model, and select the best model based on the validation set performance in the final ensemble model. The network choice in the final ensemble model is based on ablation studies using different architectures, as reported in later sections. The intuition behind the ensemble method is that, experimentally, the model with uncropped images performed better than the cropped images. This is likely due to the error introduced by the pretrained disc segmentation model that is used to crop the images. At the same time, cropped images containing the optic disc area are most important for glaucoma diagnosis, as stated in literature [15] and shown experimentally in our GradCAM visualization Figure A.1. We therefore retain both models in the final ensemble model. Lastly, in the final model, we apply polar transformation, which converts the image representation from Cartesian coordinates to polar coordinates system. For a point (u, v) in the Cartesian space, we obtain the radius r and angle θ as follows [7]:

$$\begin{cases} r = \sqrt{u^2 + v^2} \\ \theta = \tan^{-1}(\frac{v}{u}) \end{cases} \leftrightarrow \begin{cases} u = r \cos \theta \\ v = r \sin \theta \end{cases} \quad (1)$$

Figure 2 illustrates the polar transformation of the optic disc. The transformation converts the radial relationship between the optic disc, cup, and background to a spatial hierarchical structure. Therefore, this may provide an alternative view to the classification model, which can help capture more complex features. [18] claims that this transformation enhances the low level information in the optic disc region. The final classification prediction is obtained by taking

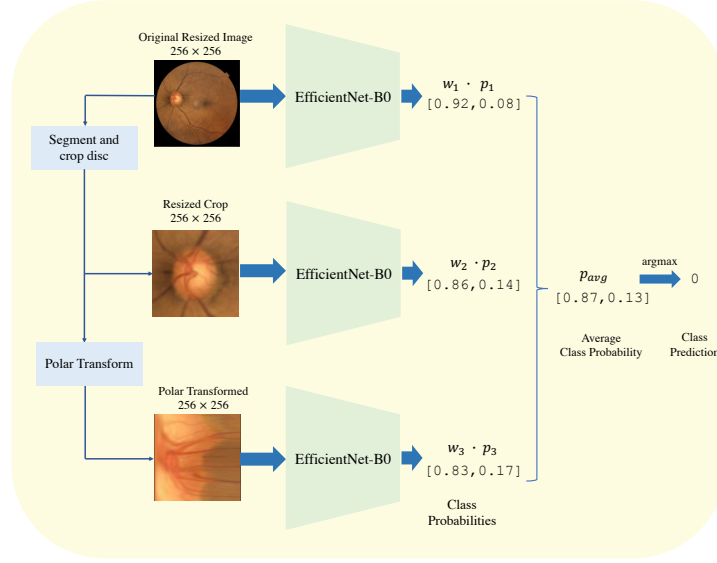


Fig. 3. Our ensemble model is composed of three different convolutional neural networks trained on different views of the color fundus images. The classification result is obtained by a weighted averaging of the class probabilities in each model. w_n refers to the weight coefficient corresponding to model n , and p_n is the soft-max probability predictions in model n .

a weighted average of the three soft-max predictions, followed by assigning the prediction label to the class that scored the highest probability.

4 Datasets

Rotterdam EyePACS AIROGS The Rotterdam EyePACS AIROGS dataset [26] consists of 113,893 color fundus images. The training set is only available to be downloaded, which has 101,442 gradable images (images of acceptable quality). The test set is not accessible to the public and has 11,000 gradable and ungradable images. Each image in the dataset is annotated by an expert as “referable glaucoma” or “no referable glaucoma”. The images are high in resolution and do vary in size. As illustrated in Figure 5, the classes are imbalanced. The size of “no referable glaucoma” (normal) class is approximately 15 times greater than the “referable glaucoma” class.

RIM-ONE DL Retinal IMage database for Optic Nerve Evaluation for Deep Learning (RIM-ONE DL) dataset [8] is used in this project as an external test dataset, which consists of 313 normal and 172 glaucomatous fundus images. All images were segmented, then cropped around the cup-disc area. There are two train/test split versions of this dataset; one was split randomly and the other

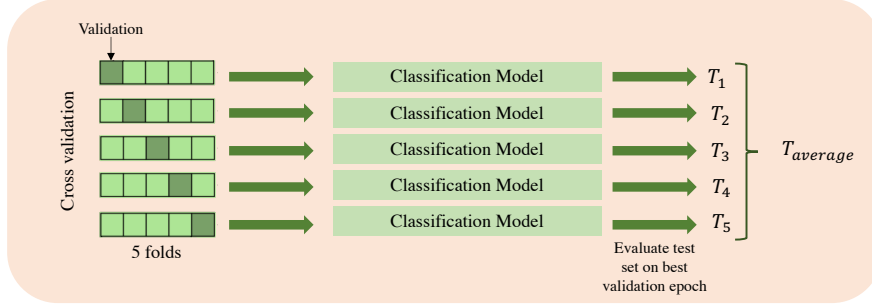


Fig. 4. 5-fold Cross-validation applied on our dataset, where T_n is the test results evaluated using the model trained on fold n and $T_{average}$ is the average test results across all $k=5$ folds.

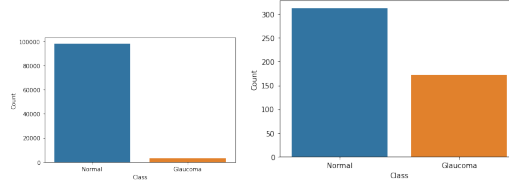


Fig. 5. Both datasets have data imbalance problem. **Left:** In the Rotterdam EyePACS AIROGS training dataset, the normal images are ~ 30 times greater than referable glaucoma. **Right:** In RIM-ONE DL dataset, the normal images are approximately twice as great as referable glaucoma.

was split by hospitals in Madrid and Zaragoza. We chose to report the results on the one split by the hospitals. The train set consists of 311 images, and the test set contains 174 images. As shown in Figure 5, the classes are also imbalanced.

5 Experimental Setup

Images have different dimensions in both datasets. Consequently, all the images are resized to 256×256 , and 512×512 for some experiments. To address the problem of the imbalanced classes in both datasets, we utilize weighted cross entropy as a loss function. The evaluation metrics used are Area Under Curve (AUC) and F-score (F1).

Rotterdam EyePACS AIROGS Our models were trained for 50 epochs on a single NVIDIA A100 GPU with a batch size of 64. An Adam optimizer was used with a learning rate ranging between 1×10^{-4} - 1×10^{-3} . These hyperparameters were chosen experimentally based on the validation results. For some experiments, we apply data augmentations consisting of random vertical flip ($p = 0.5$), random horizontal flip ($p = 0.5$) and random rotation (degrees= $(-10^\circ, +10^\circ)$).

In some of our experiments, we apply *Contrast Limited Adaptive Histogram Equalization (CLAHE)*, as inspired by previous works. The advantage of using CLAHE is that it enhances the contrasts and dampens any noise amplification [18].

Given that the original test set is not available, we split the train data into train and test splits, using approximately 90/10 percents. To validate the robustness of our models, we performed 5-fold cross-validation, as illustrated in Figure 4. The train data is split into train and validation sets, with approximately 80/20 percent. As a result, the dataset sizes for train, validation, and test are 73,154, 18,288 and 10,000, respectively.

Finally, in the ensemble model, we assign higher weight ($w = 2$) to the model trained on the original images, as it performs better on the validation set as shown in following sections. The other two models generally have similar performances, and therefore share the same weights ($w = 0.5$) when computing the overall weighted average.

RIM-ONE DL For this dataset, our main goal is to validate our model trained on the Rotterdam EyePACS AIROGS generalizability on a completely new unseen dataset. We visually noticed that the optic disc occupied a larger area in the image. We therefore retrain our best model with scaling augmentation that mimics this behavior, and results in a model invariant to images with different scales.

To fine tune our model on the RIM-ONE DL dataset, we train the model for 10 epochs with batch size of 32 using Adam optimizer with a learning rate of 1×10^{-3} and dropout rate of 0.3.

6 Experiments & Results

Rotterdam EyePACS AIROGS Table 1 shows a summary of our experiments on the Rotterdam EyePACS AIROGS dataset. On the cropped data, we performed multiple experiments using different convolutional neural networks such as EfficientNet-B0, EfficientNet-B1, MobileNet-V3, ResNet18, ResNet34, ResNet50 and DenseNet in addition to Vision Transformer (ViT-Base) with patch size 16. We experimented with several experimental hyperparameters such as dropout, applying CLAHE and augmentations. Our best performance on the cropped images was obtained with EfficientNet-B0 model with dropout ($p = 0.5$), CLAHE and augmentations, gaining an AUC of 0.87 ± 0.03 and F1-score of 0.76 ± 0.01 . To verify the performance of our cropped images vs. the original images, we trained the original images on the same model configurations as our best model, and obtained a higher AUC of 0.89 ± 0.02 and F1-score of 0.81 ± 0.02 . Additionally, we further repeated the training of the best scoring model using polar transformations, which obtained a slightly inferior performance of AUC 0.85 ± 0.02 and F1-score of 0.75 ± 0.00 . The worst performance was obtained with ViT-B_{224×224} model with an AUC score of 0.65 ± 0.05 and F1-score of 0.57 ± 0.04 .

Table 1. Experimental results on the Rotterdam EyePACS AIROGS dataset. D =dropout, A =augmentations, C =CLAHE, S =scaling transformation. EfficientNet-B0_{original} refers to EfficientNet-B0 model trained on the original (uncropped) data.

ID	Model	Test AUC	Test F-1
1	ViT-B _{224×224} (D,A,C)	0.65 ± 0.05	0.57 ± 0.04
2	Resnet18	0.75 ± 0.02	0.72 ± 0.01
3	Resnet34	0.76 ± 0.02	0.73 ± 0.00
4	Resnet34 (C)	0.76 ± 0.02	0.74 ± 0.01
5	ViT-B _{224×224}	0.77 ± 0.04	0.67 ± 0.01
6	Resnet50	0.78 ± 0.02	0.70 ± 0.02
7	DenseNet-121	0.79 ± 0.03	0.71 ± 0.02
8	EfficientNet-B1	0.79 ± 0.01	0.78 ± 0.01
9	EfficientNet-B0	0.80 ± 0.03	0.77 ± 0.01
10	MobileNet-V3 Large	0.81 ± 0.01	0.77 ± 0.03
11	EfficientNet-B0 (D,A,C,P)	0.85 ± 0.02	0.75 ± 0.00
12	EfficientNet-B0 (A,C)	0.85 ± 0.02	0.76 ± 0.01
13	MobileNet-V3 Large (D,A,C)	0.87 ± 0.02	0.72 ± 0.02
14	EfficientNet-B0 (D,A,C,S)	0.87 ± 0.02	0.76 ± 0.02
15	EfficientNet-B0 (D,A,C)	0.87 ± 0.03	0.76 ± 0.01
16	EfficientNet-B0 _{original} (D,A,C)	0.89 ± 0.02	0.81 ± 0.02
17	Ensemble (#11, #15, #16)	0.92	0.80

RIM-ONE DL Table 2 summarizes our test results on the RIM-ONE DL dataset using different fractions of the train set to fine-tune on our best model (Experiment ID #14). As we may note, the experiment with no fine-tuning performs the worst, scoring an AUC score of 0.78 and F1-Score of 0.75. When we introduce 50% of the train data for fine-tuning, the AUC score significantly improves to 0.91 and the F1-score to 0.90. As we further increase the size of the fine-tune data beyond 50%, we don’t observe more improvements.

Table 2. Experimental results on RIM-One DL dataset.

Model	% train data	Model Init	Test AUC	Test F-1
VGG19 [8]	100	ImageNet	0.92	-
EfficientNet-B0	100	ImageNet	0.72	0.75
EfficientNet-B0	0	#14	0.78	0.75
EfficientNet-B0	25	#14	0.87	0.88
EfficientNet-B0	50	#14	0.91	0.90
EfficientNet-B0	100	#14	0.90	0.88

7 Discussion

Our results indicate that the models trained on the uncropped images performed much better than the cropped images. We hypothesize that this is due to errors

introduced by the pretrained disc segmentation model that is used to crop the images. As we previously stated, approximately 20% of our data failed to segment the optic disc using this model. Furthermore, our experiments show that using dropout improves the performance, and therefore is a good strategy for overfitting. Additionally, using augmentations and CLAHE on top of dropout significantly improves the performance. By using augmentations and CLAHE, we increase the effective dataset size and also overcome model overfitting, making it robust to spatial and color transformations.

Furthermore, the ViT-B model did not perform as good as the EfficientNet-B0 model. The Vision Transformer model requires a large amount of data to perform as well as CNNs, therefore we can hypothesize that its inferior performance is due to the small number of training samples. As compared to the experiments in [6], the dropout value we assigned was too high, which might have negatively impacted the result. In addition, ResNet models with less number of layers performed worse, as smaller models are not able to capture the complex features in our dataset.

For the RIM-ONE DL experiments, we can conclude that RADNet generalizes well on this dataset when fine-tuned on a small fraction of the train dataset for a few epochs. We further report the results using a VGG19 model as listed in [8]. Furthermore, we tested a similar architecture and experimental configurations with ImageNet weights, which provided an inferior performance when compared to testing it with our pretrained model.

Lastly, the ensemble model outperformed all previous experiments. By combining our three best performing CNNs, each trained on a different view of the same data, we achieve an AUC of 0.92. Furthermore, we give more classification decision weight to the best performing CNN, Experiment 17 (Table 1), which helped achieve this performance.

8 Conclusion

In this paper, we introduced an ensemble model RADNet for glaucoma classification composed of three different CNNs trained on different views of the color fundus images. We trained our model on the AIROGS dataset and tested our results on a subset of that dataset in addition to an external dataset, RIM-ONE DL. Our results indicate that an ensemble model significantly improves the performance when compared to individual models. Furthermore, when testing our data on the external dataset, we get comparable performance to the previous state of the art after fine-tuning the model to a fraction of the train dataset. In future works, we would like to extend the weighted averaging of the ensemble model predictions, such that the weights are determined systematically rather than being constant. Additionally, we would like to evaluate the performance of RADNet using smaller fractions of the train dataset, to understand the impact of dataset size to our model performance.

References

1. Allison, K., Patel, D., Alabi, O.: Epidemiology of Glaucoma: The Past, Present, and Predictions for the Future. *Cureus* (Nov 2020). <https://doi.org/10.7759/cureus.11686>, <https://www.cureus.com/articles/42672-epidemiology-of-glaucoma-the-past-present-and-predictions-for-the-future>
2. Camara, J., Neto, A., Pires, I.M., Villasana, M.V., Zdravevski, E., Cunha, A.: Literature Review on Artificial Intelligence Methods for Glaucoma Screening, Segmentation, and Classification. *Journal of Imaging* **8**(2), 19 (Jan 2022). <https://doi.org/10.3390/jimaging8020019>, <https://www.mdpi.com/2313-433X/8/2/19>
3. Chollet, F.: Xception: Deep learning with depthwise separable convolutions. In: *Proceedings of the IEEE conference on computer vision and pattern recognition*. pp. 1251–1258 (2017)
4. Conlon, R., Saheb, H., Ahmed, I.I.K.: Glaucoma treatment trends: a review. *Canadian Journal of Ophthalmology* **52**(1), 114–124 (Feb 2017). <https://doi.org/10.1016/j.jcjo.2016.07.013>, <https://linkinghub.elsevier.com/retrieve/pii/S0008418216300758>
5. Dibia, A.C., Nwawudu, S.E.: Automated detection of glaucoma from retinal images using image processing techniques **7**, 2321–9009 (09 2018)
6. Dosovitskiy, A., Beyer, L., Kolesnikov, A., Weissenborn, D., Zhai, X., Unterthiner, T., Dehghani, M., Minderer, M., Heigold, G., Gelly, S., Uszkoreit, J., Houlsby, N.: An image is worth 16x16 words: Transformers for image recognition at scale. *CoRR* **abs/2010.11929** (2020), <https://arxiv.org/abs/2010.11929>
7. Fu, H., Cheng, J., Xu, Y., Wong, D.W.K., Liu, J., Cao, X.: Joint optic disc and cup segmentation based on multi-label deep network and polar transformation. *IEEE Transactions on Medical Imaging* **37**(7), 1597–1605 (jul 2018). <https://doi.org/10.1109/tmi.2018.2791488>, <https://doi.org/10.1109%2Ftmi.2018.2791488>
8. Fumero, F., Diaz-Aleman, T., Sigut, J., Alayón, S., Arnay, R., Angel-Pereira, D.: Rim-one dl: A unified retinal image database for assessing glaucoma using deep learning. *Image Analysis and Stereology* **39** (10 2020). <https://doi.org/10.5566/ias.2346>
9. Fumero, F., Sigut, J., Alayón, Silvia andGonzález-Hernández, M., González de la Rosa, M.: Interactive tool and database for optic disc and cup segmentation of stereo and monocular retinal fundus images (06 2015)
10. Huang, G., Liu, Z., Van Der Maaten, L., Weinberger, K.Q.: Densely connected convolutional networks. In: *Proceedings of the IEEE conference on computer vision and pattern recognition*. pp. 4700–4708 (2017)
11. Iandola, F.N., Han, S., Moskewicz, M.W., Ashraf, K., Dally, W.J., Keutzer, K.: SqueezeNet: Alexnet-level accuracy with 50x fewer parameters and < 0.5 mb model size. *arXiv preprint arXiv:1602.07360* (2016)
12. Khan, S.M., Liu, X., Nath, S., Korot, E., Faes, L., Wagner, S.K., Keane, P.A., Sebire, N.J., Burton, M.J., Denniston, A.K.: A global review of publicly available datasets for ophthalmological imaging: barriers to access, usability, and generalisability. *The Lancet Digital Health* **3**(1), e51–e66 (Jan 2021). [https://doi.org/10.1016/S2589-7500\(20\)30240-5](https://doi.org/10.1016/S2589-7500(20)30240-5), <https://linkinghub.elsevier.com/retrieve/pii/S2589750020302405>
13. Krizhevsky, A., Sutskever, I., Hinton, G.E.: Imagenet classification with deep convolutional neural networks. In: Pereira, F., Burges, C., Bottou, L., Weinberger, K. (eds.) *Advances in Neural Information Processing Systems*. vol. 25. Curran Associates, Inc. (2012), <https://proceedings.neurips.cc/paper/2012/file/c399862d3b9d6b76c8436e924a68c45b-Paper.pdf>

14. Lee, D.A., Higginbotham, E.J.: Glaucoma and its treatment: A review. *American Journal of Health-System Pharmacy* **62**(7), 691–699 (Apr 2005). <https://doi.org/10.1093/ajhp/62.7.691>, <https://academic.oup.com/ajhp/article/62/7/691/5134357>
15. Lee, J., Lee, J., Song, H., Lee, C.: Development of an end-to-end deep learning system for glaucoma screening using color fundus images. *JAMA Ophthalmol.* **137**, 1353–1360 (2019)
16. Maadi, F., Faraji, N., Bibalan, M.H.: A Robust Glaucoma Screening Method for Fundus Images Using Deep Learning Technique. In: 2020 27th National and 5th International Iranian Conference on Biomedical Engineering (ICBME). pp. 289–293. IEEE, Tehran, Iran (Nov 2020). <https://doi.org/10.1109/ICBME51989.2020.9319434>, <https://ieeexplore.ieee.org/document/9319434/>
17. Panda, R., Puhan, N.B., Mandal, B., Panda, G.: GlaucoNet: Patch-Based Residual Deep Learning Network for Optic Disc and Cup Segmentation Towards Glaucoma Assessment. *SN Computer Science* **2**(2), 99 (Apr 2021). <https://doi.org/10.1007/s42979-021-00491-1>, <http://link.springer.com/10.1007/s42979-021-00491-1>
18. Phasuk, S., Poopresert, P., Yaemsuk, A., Suvannachart, P., Itthipanichpong, R., Chansangpetch, S., Manassakorn, A., Tantisevi, V., Rojanapongpun, P., Tantibundhit, C.: Automated glaucoma screening from retinal fundus image using deep learning. In: 2019 41st Annual International Conference of the IEEE Engineering in Medicine and Biology Society (EMBC). pp. 904–907 (2019). <https://doi.org/10.1109/EMBC.2019.8857136>
19. Sandler, M., Howard, A., Zhu, M., Zhmoginov, A., Chen, L.C.: Mobilenetv2: Inverted residuals and linear bottlenecks. In: Proceedings of the IEEE conference on computer vision and pattern recognition. pp. 4510–4520 (2018)
20. Selvaraju, R.R., Das, A., Vedantam, R., Cogswell, M., Parikh, D., Batra, D.: Gradcam: Why did you say that? visual explanations from deep networks via gradient-based localization. *CoRR abs/1610.02391* (2016), <http://arxiv.org/abs/1610.02391>
21. Sevastopolsky, A.: Optic disc and cup segmentation methods for glaucoma detection with modification of u-net convolutional neural network. *Pattern Recognition and Image Analysis* **27**(3), 618–624 (jul 2017). <https://doi.org/10.1134/s1054661817030269>, <https://doi.org/10.1134/2Fs1054661817030269>
22. Sreng, S., Maneerat, N., Hamamoto, K., Win, K.Y.: Deep Learning for Optic Disc Segmentation and Glaucoma Diagnosis on Retinal Images. *Applied Sciences* **10**(14), 4916 (Jul 2020). <https://doi.org/10.3390/app10144916>, <https://www.mdpi.com/2076-3417/10/14/4916>
23. Szegedy, C., Ioffe, S., Vanhoucke, V., Alemi, A.A.: Inception-v4, inception-resnet and the impact of residual connections on learning. In: Thirty-first AAAI conference on artificial intelligence (2017)
24. Szegedy, C., Vanhoucke, V., Ioffe, S., Shlens, J., Wojna, Z.: Rethinking the Inception Architecture for Computer Vision. In: 2016 IEEE Conference on Computer Vision and Pattern Recognition (CVPR). pp. 2818–2826. IEEE, Las Vegas, NV, USA (Jun 2016). <https://doi.org/10.1109/CVPR.2016.308>, <http://ieeexplore.ieee.org/document/7780677/>
25. Szegedy, C., Wei Liu, Yangqing Jia, Sermanet, P., Reed, S., Anguelov, D., Erhan, D., Vanhoucke, V., Rabinovich, A.: Going deeper with convolutions. In: 2015 IEEE Conference on Computer Vision and Pattern Recognition (CVPR). pp. 1–9. IEEE, Boston, MA, USA (Jun 2015). <https://doi.org/10.1109/CVPR.2015.7298594>, <http://ieeexplore.ieee.org/document/7298594/>

26. Coen de Vente, Koenraad A. Verrmeer, N.J.B.v.G.H.G.L.C.I.S.: Airops: Artificial intelligence for robust glaucoma screening challenge. In: IEEE International Symposium on Biomedical Imaging. Ieee (2022)
27. Zhang, X., Zhou, X., Lin, M., Sun, J.: Shufflenet: An extremely efficient convolutional neural network for mobile devices. In: Proceedings of the IEEE conference on computer vision and pattern recognition. pp. 6848–6856 (2018)
28. Zoph, B., Vasudevan, V., Shlens, J., Le, Q.V.: Learning transferable architectures for scalable image recognition. In: Proceedings of the IEEE conference on computer vision and pattern recognition. pp. 8697–8710 (2018)

A Supplementary Material

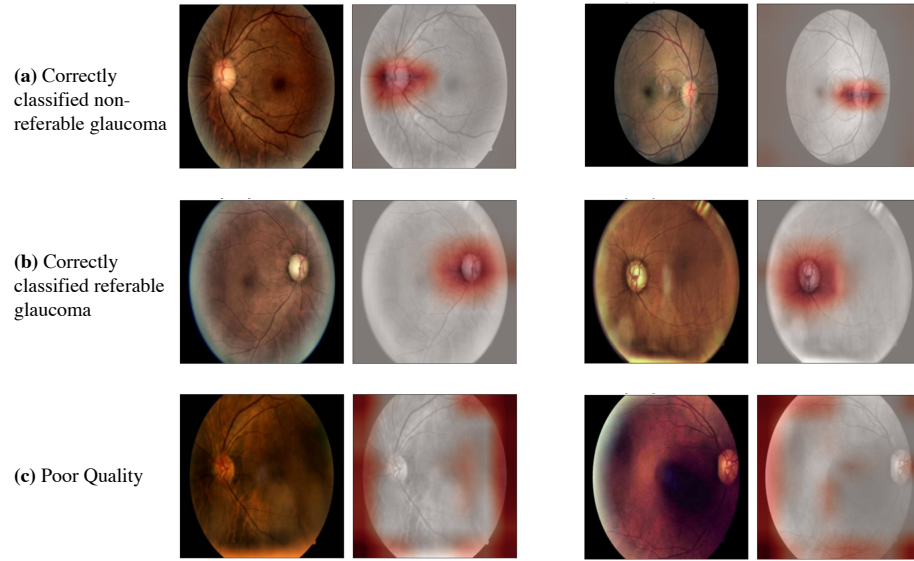


Fig. A.1. GradCAM [20] visualization on EfficientNet-B0 model trained on the uncropped AIROGS dataset.